Gondwana Research 85 (2020) 224–236

Contents lists available at ScienceDirect

Gondwana Research

journal homepage: www.elsevier.com/locate/gr

Large Zn isotope variations in the Ni—Mo polymetallic sulfide layer in the lower Cambrian, South China

Haifeng Fan [a,b,*], Hongjie Zhang [a,b], Chaoyi Xiao [a,b], Jan Pašava [c], Tao Han [a,b], Ting Zhou [a,b], Hanjie Wen [a,b]

[a] State Key Laboratory of Ore Deposit Geochemistry, Institute of Geochemistry, Chinese Academy of Sciences, Guiyang 550002, China
[b] University of Chinese Academy of Sciences, Beijing 100049, China
[c] Czech Geological Survey, Geologická 6, 152 00 Praha 5, Czech Republic

ARTICLE INFO

Article history:
Received 14 November 2019
Received in revised form 27 April 2020
Accepted 29 April 2020
Available online 9 June 2020

Handling Editor: F. Pirajno

Keywords:
Zn isotopes
Zn source
Ni—Mo polymetallic sulfide layer
Hydrothermal fluids

ABSTRACT

In South China, black organic-rich shales in the lower Cambrian Niutitang Formation host a Ni—Mo polymetallic sulfide layer that discontinuously extends over ~1600 km. Seawater and hydrothermal origins are among the many suggested hypotheses and are still under debate. In order to discriminate Zn sources, we report Zn isotopes in Ni—Mo polymetallic sulfide layers and their host shales from the Nayong and Zunyi locations in Guizhou province and the Zhangjiajie section in Hunan province. In each section, host organic-rich shales show homogeneous Zn isotope compositions which likely resulted from quantitative scavenging of dissolved Zn from seawater under euxinic conditions. The difference in the average δ^{66}Zn values of organic-rich shales between the two sections in Guizhou (0.76 ± 0.09‰) and one section in Hunan (0.59 ± 0.10‰) might reflect variations of Zn isotope gradient with the depth of seawater. Therefore, the organic-rich sediments need not always represent an isotopically light Zn sink, which is dependent on Zn isotope fractionation in the local basin. However, the δ^{66}Zn values in the Ni—Mo polymetallic sulfide layers are different from those of their host shales, indicating that these sulfide layers did not inherit the Zn isotope signal of seawater. Based on the regular increasing trend in δ^{66}Zn values from Nayong (0.54 ± 0.06‰) to Zhangjiajie (1.34 ± 0.09‰) and the presence of Pb—Zn mineralization in the Dengying/Doushantuo Formations, we argue that hydrothermal fluids associated with Pb—Zn mineralization could be a major source of Zn in Ni—Mo sulfide layers, especially in the Nayong location. A possible model is that the hydrothermal fluids related to MVT-type mineralization got overprinted on a multiple-sourced synsedimentary sulfide-rich layer. We provide additional evidence that Zn isotopes have great potential as a tracer of metal source and can be applied to similar types of mineralization as e.g., the late Devonian Ni-Zn-PGE Nick deposit (Selwyn Basin, Canada) or elsewhere.

1. Introduction

Organic-rich shales (black shales) commonly contain economically significant concentrations of metals. Examples include the Paleoproterozoic Ni-Cu-Zn-Co deposit at Talvivaara in Finland (Loukola-Ruskeeniemi and Lahtinen, 2013), the Neoproterozoic Sukhoi Log gold deposit in Russia (Distler et al., 2004), the Lower Devonian Sn-polymetallic deposits in the Dachang tin field in south China (Pašava et al., 2003), the Late Devonian Ni—Zn at Nick property in Selwyn Basin at Yukon in Canada (Orberger et al., 2003), the Permian Cu—Ag deposit of the Kupferschiefer type in Poland (Oszczepalski, 1989), and others. In south China, the transgressive black shale sequence is distributed over more than ~1600 km along the rifted margin of the southeastern Yangtze platform during the early Cambrian (Tommotian) (e.g., Chen et al., 1982; Fan, 1983; Coveney Jr. and Chen, 1991; Steiner et al., 2001; Mao et al., 2002). A few-centimeter-thick (1–30 cm) sulfide mineralization, known as Ni—Mo polymetallic sulfide layer, was discovered in the lower Cambrian black shales (Niutitang Formation) about 40 years ago (Chen et al., 1982; Fan, 1983). This Ni—Mo polymetallic sulfide layer is exceptionally enriched in Mo and Ni (up to 9%), and Se-Re-As-Hg-Sb-Tl (>1000 times enriched relative to bulk continental crust), and platinum group elements (PGE > 100 times enriched relative to bulk continental crust) (e.g., Chen et al., 1982; Fan, 1983; Steiner et al., 2001; Mao et al., 2002). One such locality – the Huangjiawan deposit, located ~15 km west of Zunyi, Guizhou – contains ore reserves of 240,000 t Mo + 150,000 t Ni (Mao et al., 2002).

The metal origin in the Ni—Mo polymetallic sulfide layer has been much debated. Most models explain the metal enrichment by submarine hydrothermal fluid discharge (e.g., Coveney Jr. et al., 1994, Coveney Jr., 2003; Lott et al., 1999; Steiner et al., 2001; Jiang et al., 2007), seawater scavenging (Mao et al., 2002; Lehmann et al., 2003, 2007, 2016; Xu et al., 2013; Pagès et al., 2018), and multiple sources

* Corresponding author at: State Key Laboratory of Ore Deposit Geochemistry, Institute of Geochemistry, Chinese Academy of Sciences, Guiyang 550002, China.
E-mail address: fanhaifeng@mail.gyig.ac.cn (H. Fan).

https://doi.org/10.1016/j.gr.2020.04.009
1342-937X/

by mixing seawater with hydrothermal fluid and terrestrial weathering products (Jiang et al., 2006; Pašava et al., 2008, 2018; Han et al., 2015), although an extraterrestrial impact origin has also been proposed (Fan et al., 1984; Coveney Jr. et al., 1992). Many studies suggested that redox conditions of seawater played an important role in concentrating metals (e.g., Murowchick et al., 1994; Jiang et al., 2007; Lehmann et al., 2016; Pagès et al., 2018). More recently, multiple metal isotopes have also been applied to constrain the source of various metals in the sulfide layer. For examples, Mo, Cr and Hg isotopes confirmed the seawater scavenging hypothesis as before by Os isotope (Lehmann et al., 2007, 2016; Xu et al., 2011; Loukola-Ruskeeniemi and Lahtinen, 2013; Yin et al., 2017). Selenium and Ni isotopes indicated hydrothermal inputs for Se (Wen and Carignan, 2011), and ultra-mafic and malfic-rock weathering sources for Ni, respectively (Pašava et al., 2018). Following these new proxies, it is most likely that enriched metals in the Ni—Mo polymetallic sulfide layer were derived from different sources. In this multiple-sources model, Zn-Ni-Sb-V-PGE have been suggested to come from submarine hydrothermal fluids, while a seawater origin was proposed for Mo and Tl (e.g., Orberger et al., 2007; Pašava et al., 2008; Han et al., 2015).

It is noted that Zn concentrations show local enrichment and regular variations in these sulfide layers. For example, an extreme Zn enrichment (average of 4.8 wt%) has been observed in the location of southwestern of Guizhou province (Zhijin and Nayong) and north-eastern of Yunnan province (Deze), compared to that of Zunyi (3000 ppm–5000 ppm) in Guizhou province and Zhangjiajie (145–5000 ppm) areas in Hunan province (e.g., Chen et al., 1982; Xu et al., 2012; Han et al., 2015). Recently, Zn isotopes have been successfully used to monitor precipitation processes in hydrothermal mineralization, and provide new insights into the genesis of ore systems including Pb—Zn ore deposits. Recent studies of Zn isotopes in hydrothermal systems suggest that light Zn isotopes are preferentially incorporated in early-deposited sulfides at deeper/hotter parts of the hydrothermal system, however, while residual fluid and late-precipitated sphalerite have heavy Zn isotopic composition (e.g., Mason et al., 2005; Wilkinson et al., 2005; John et al., 2008; Kelley et al., 2009; Gagnevin et al., 2012), although other factors (e.g., pH) could also impact Zn isotope variations (Pašava et al., 2014). The evolution from light to heavy Zn isotopic composition could be attributed to Raleigh fractionation during migration of hydrothermal fluids (e.g., Wilkinson et al., 2005; Kelley et al., 2009). Therefore, a similar increasing trend in Zn isotopes controlled by Raleigh fractionation may be observed in these sulfide layers if metal Zn is sourced from the same hydrothermal fluids. In contrast, if metal Zn in all sulfide layers was derived from seawater, homogenous Zn isotopic composition should be recorded, since modern and Ediacaran deep water are shown to have homogenous Zn isotope compositions (0.50 ± 0.14‰, Maréchal et al., 2000; Little et al., 2014; Fan et al., 2018).

Here, we use Zn isotopes combined with trace element data to discriminate between the seawater scavenging and submarine hydrothermal fluid discharge models for the source of Zn. We investigated three Ni—Mo polymetallic sulfide layers and their host black shales from the Nayong and Zunyi sections in Guizhou province, and the Zhangjiajie section in Hunan province. Based on our new data, a local hydrothermal metal source is required to explain Zn enrichment in the lower Cambrian Ni—Mo polymetallic sulfide layers hosted in the Niutitang Formation on the Yangtze platform.

2. Geological setting

During the early Cambrian, South China was an isolated craton consisting of the Yangtze and Cathaysia blocks, and the Nanhua Basin (Wang and Li, 2003). The sedimentary successions in the Nanhua Basin were deposited in a passive continental margin of the Yangtze Platform. There are four distinct sedimentary facies belts from northwest to southeast direction: Carbonate platform, protected basin, Jiangnan uplift and deep basin (Fig. 1, Steiner et al., 2001). The shallow

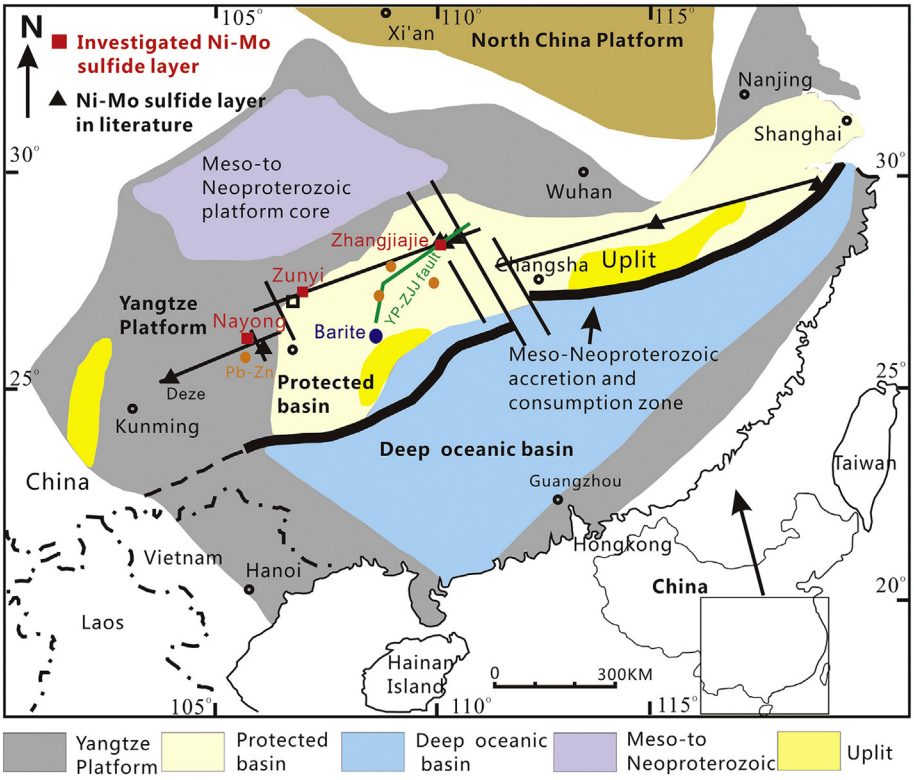

Fig. 1. Geological setting and distribution of Ni—Mo polymetallic sulfide layers in the Niutitang Formation, South China, early Cambrian, modified from Steiner et al. (2001). Seawater depth in the Nayong and Zunyi sections is about less than 100 m, however, that of the Zhangjiajie section is >100 m. There is possibly a major synsedimentary fault system parallel to the Early Neoproterozoic island arc along a narrow linear belt. YP-ZJJ: Yuping-Zhangjiajie.

water platform is characterized by the Meishucun Formation dolostone and interbedded dolostone and phosphorite. Deep-water slope and basin contain mainly black chert (part of the Liuchapo Formation) and transgressive black shale successions (the Niutitang Formation). These black shales host discontinuous polymetallic Ni—Mo sulfide layers extending over ~1600 km belt from Yunnan to Zhejiang province (Fig. 1, Fan et al., 1984), which grades laterally into vanadium deposits in Guizhou, Hunan, Hubei, Jiangxi and Zhejiang provinces (e.g., Lehmann et al., 2016). This belt possibly represents a major southwest (SW)-northeast (NE) deep fault zone in the transitional area between Neoproterozoic back-arc basin and platform (Steiner et al., 2001). Those deep-water cherts host major barite ore deposits in Guizhou and Hunan provinces, which may be contemporaneous to the Ni—Mo sulfide layers (e.g., Jiang et al., 2007; Pašava et al., 2008). In addition, other mineralization occurrences are also present in the Nayong area, such as the Pb—Zn deposits, in the Neoproterozoic Dengying Formation (Tan et al., 2012; Han et al., 2015). Along the Yuping-Zhangjiajie fault, there are also numerous Pb—Zn deposits hosted in the Neoproterozoic Doushantuo Formation dolostone overlain by the Dengying Formation, such as Dongjiahe, Dilu Pb—Zn ore deposits (Duan, 2014 and reference therein).

The three main study sections are the Nayong and Zunyi sections in Guizhou province, and the Zhangjiajie section in Hunan province. In all three areas, black shales of the Lower Cambrian Niutitang Formation are underlain primarily by the dolostone of the Neoproterozoic Dengying Formation or chert of the Liuchapo Formation, and overlain by greenish shale, siltstone and fine-grained sandstone of the Mingxinsi Formation. The lower Cambrian Niutitang Formation exhibits a similar lithological stratigraphy composition from the bottom to the top (e.g., Steiner et al., 2001; Xu et al., 2011; Fan et al., 2011, 2013; Han et al., 2015; Lehmann et al., 2016). The detailed stratigraphic sequence (Fig. 2) comprises: (1) A clay layer (0.1–0.5 m thick) unconformably overlying the karst paleosurface of dolostone of the Dengying Formation in the Nayong section; (2) A phosphorite layer (0–0.5 m thick) in all three sections; (3) A volcanic tuff (0–0.3 m thick) with a SHRIMP U—Pb zircon ages of 532.3 ± 0.7 Ma (Jiang et al., 2009) in the Zunyi section and of 536.3 ± 5.5 Ma in the Zhangjiajie area (Chen et al., 2009); (4) A bedded chert commonly intercalated with black shale (0–2 m thick) in the Zunyi area and a thick chert layer in the Zhangjiajie area; (5) The lower black shale (0–8 m thick); (6) A black coarse-grained limestone concretion in the Nayong and Zunyi sections; (7) The Ni—Mo polymetallic sulfide layer (0.02–0.6 m thick) that has a Re—Os isochron age of 521 ± 5 Ma (Xu et al., 2011); (8) The upper black shale (≥20 m thick).

3. Samples and methods

3.1. Samples

The studied samples include Ni—Mo polymetallic sulfide layers and host black shales from the Nayong, Zunyi and Zhangjiajie sections (Fig. 2). Both the Ni—Mo sulfide layers and host black shales contain abundant total organic carbon (TOC), up to 15 wt% (e.g., Steiner et al., 2001; Orberger et al., 2007). Organic material is commonly brecciated pyrobitumen (Kříbek et al., 2007). In the host black shales, Zn mainly exists as sphalerite (Kao et al., 2001; Orberger et al., 2007; Han et al., 2014), there is no significant correlation between Zn and TOC concentrations (Han et al., 2015). The major minerals in Ni—Mo sulfide layers, i.e. MoSC phase (the complex of Mo-sulfide and carbonaceous matter), millerite, sphalerite and pyrite, are present as rounded and brecciated clasts and nodules in the silicate matrix (e.g., Kao et al., 2001; Steiner et al., 2001; Han et al., 2014; Han et al., 2015). Although previous studies suggest that MoSC phase has high Zn concentrations (800 ppm, Orberger et al., 2007) and Zn is dispersed and associated within organic material (Pagès et al., 2018), we observed Zn bound only to sulfides with two types of zinc mineralization labeled as Zn sulfide-1 and -2. The early-stage Zn sulfide-1 mainly occurs as fine-grained sphalerite mostly associated with Ni-sulfide grains, and shows a laminated texture (Fig. 3), which can be observed in all three studied sections. Locally, these minerals of Zn sulfide-1 replaces the MoSC and apatite, showing brecciated structure (Fig. 3). The late-stage Zn sulfide-2 is usually represented by veinlets crosscutting the earlier-formed mineral aggregates

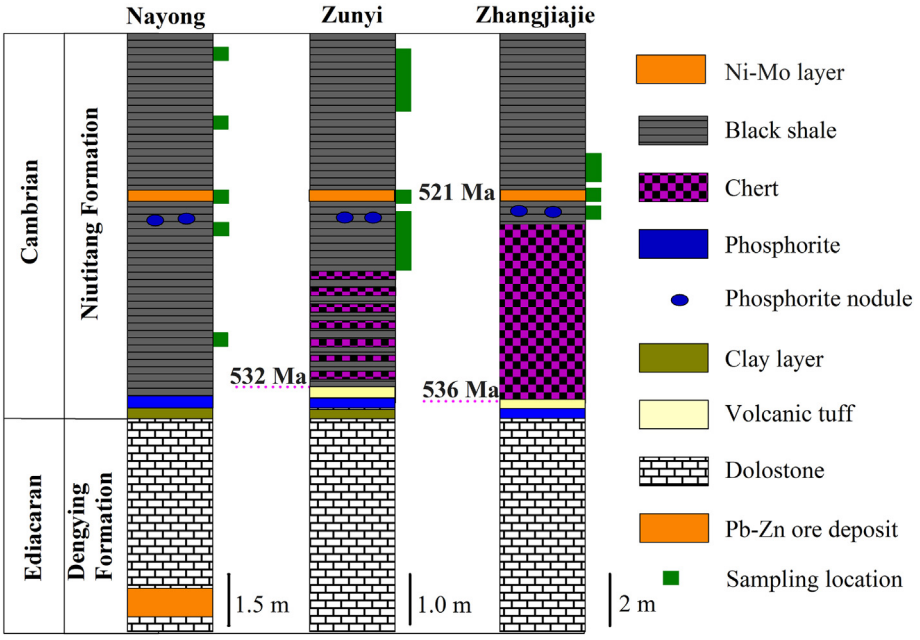

Fig. 2. Generalized stratigraphic column of the Nayong and Zunyi sections (Guizhou Province) modified from Han et al. (2015) and Fan et al. (2011) and the Zhangjiajie section (Hunan Province) modified from Fan et al. (2013).

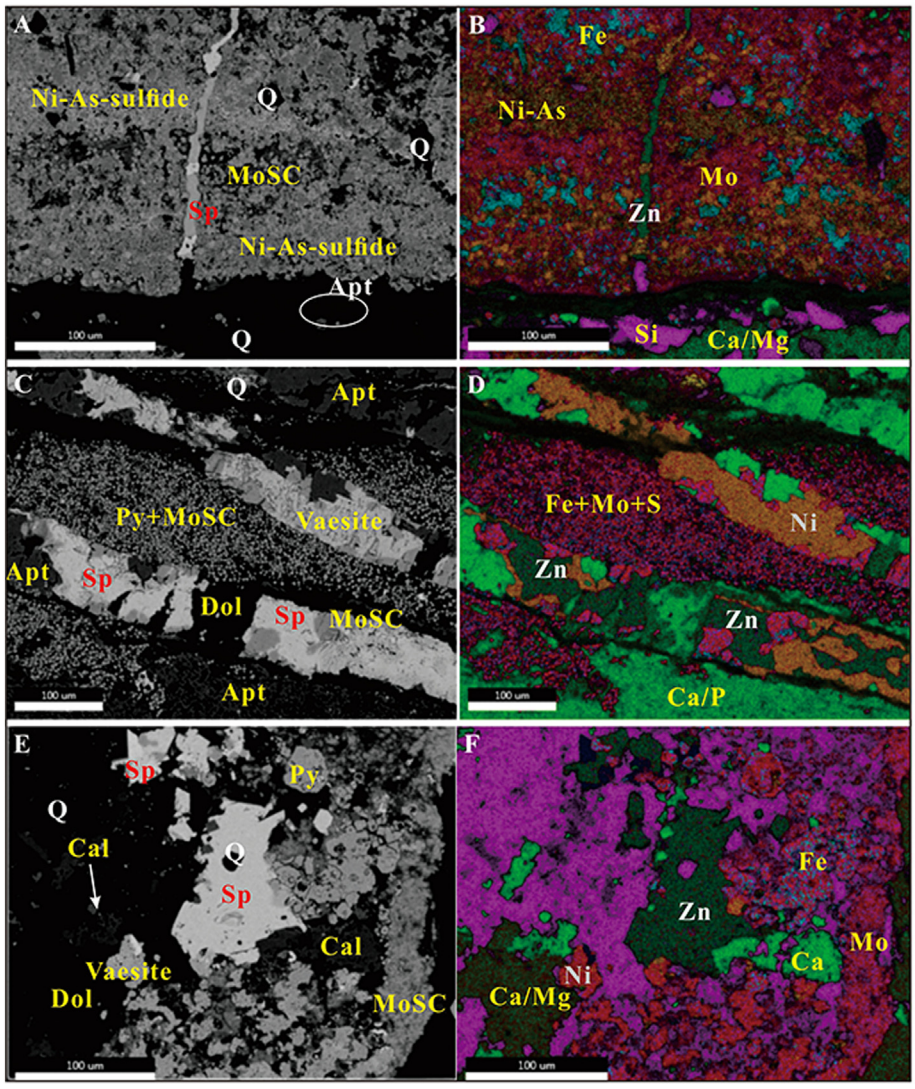

Fig. 3. SEM images of polished thin sections of Ni—Mo polymetallic sulfide layers in the Nayong (A, B), Zunyi (C, D) and Zhangjiajie (E, F) sections. Abbreviations: Apt = apatite; Cal = calcite; Dol = dolomite; MoSC = the complex of Mo-sulfide and carbonaceous matter; Py = pyrite; Q = quartz; Sp = sphalerite. SEM images were performed using a JEOL JSM-7800FX field emission scanning electronic microscope (FESEM) at the State Key Laboratory of Ore Deposit Geochemistry, Institute of Geochemistry, Chinese Academy of Sciences (IGCAS).

(Fig. 3), which is commonly observed in all sections (Orberger et al., 2007; Han et al., 2014).

3.2. Methods

3.2.1. Authigenic Zn isotope analysis

The powdered samples were digested in a Microwave device using aqua regia for 2 h or high-pressure Teflon bombs with concentrated HNO_3 at 120 °C for 24 h, to leach authigenic Zn phase. The dissolved fraction was separated from residual materials by centrifuge. Subsequently, the solution was dried on a hotplate, and then 1 mL 2 N HCl + 0.001% H_2O_2 was added to each leached fraction prior to chemical purification of Zn. AGMP-1 anion exchange resin (100–200 mesh) was used for Zn purification, following the method outlined by Tang et al. (2006). Zn concentrations and isotopic ratios were measured using a Neptune MC-ICP-MS at the Institute of Geochemistry, Chinese Academy of Sciences (IGCAS, Guiyang) during which instrumental mass bias was corrected using the IRMM3702 reference material. USGS standard reference NOD-P-1, NOD-A-1 and NIST 683 were also measured along with unknown samples to estimate external precision and accuracy. All reported $\delta^{66}Zn$ values are relative to JMC Lyons Zn solution standard, based on the published difference between $Zn_{IRMM3702}$ and $Zn_{JMC\ Lyons}$ ($\Delta^{66}Zn_{IRMM3702\text{-}JMC\ Lyons} = +0.30‰$, Vance et al., 2016). All results of standard references are consistent with previously published values (Table 1). The total combined uncertainty (2 SD) based on the long-term reproducibility of $\delta^{66}Zn$ was 0.04‰ for NIST 863.

3.2.2. Element measurement

Major element concentrations (Al and Fe) were measured by X-ray fluorescence spectrometer (XRF) at the ALS Chemex (Guangzhou) Company Limited. Trace element (including authigenic Zn) concentrations were analyzed by ICP-MS at the State Key Laboratory of Ore Deposit Geochemistry, IGCAS (Guiyang). About 50 mg of sample powder was dissolved in high-pressure Teflon bombs with HF and HNO_3 at 190 °C for 48 h. The appropriate amount of Rh was used as an internal standard to monitor drift during the analysis. The analytical precision was better than 5% for trace elements based on the long-term results of three standard reference materials (AGV-2, NOD-P-1 and NOD-A-1).

The enrichment factors (EF) of Mo and U were calculated using the following equation: $X_{EF} = (X/Al)_{sample}/(X/Al)_{PAAS}$ (Tribovillard et al., 2006, 2012; Algeo and Tribovillard, 2009) where X is equal to the weight percent concentrations of elements Mo and U, respectively and

PAAS represents the post-Archean average shale (PAAS) composition from Taylor and McLennan (1985).

4. Results

4.1. Zinc concentrations and isotope compositions

Authigenic zinc concentrations in all host black shales vary widely (Table 1 and Fig. 4A). The largest range (42–771 ppm) is observed in the Zunyi black shales. However, the Nayong and Zhangjiajie host black shales show relatively narrow ranges of Zn concentrations, from 192 ppm to 369 pm and from 125 ppm to 181 ppm, respectively. Compared to these host black shales, all Ni—Mo sulfide layers are typical of anomalous Zn values ranging from 931 ppm to 14.8 wt% (Table 1 and Fig. 4B). The highest Zn concentrations were observed in the Ni—Mo sulfide layer from the Nayong section, with the largest range from 3644 ppm to 14.8 wt%. In the Zunyi section, Zn concentrations in Ni—Mo sulfide layer are from 1820 ppm to 2424 ppm. In the Zhangjiajie section, Zn concentrations in Ni—Mo sulfide layer range from 931 ppm to 6590 ppm.

All host black shales from the three studied sections exhibit relatively varied Zn isotope compositions, ranging from 0.47‰ to 0.94‰ (Table 1 and Fig. 4A). For example, the δ^{66}Zn values change from 0.59‰ to 0.94‰ in the Nayong section (average 0.73 ± 0.12‰), from 0.71‰ to 0.89‰ in the Zunyi section (average 0.78 ± 0.05‰), and from 0.47‰ to 0.77‰ in the Zhangjiajie section (average 0.59 ± 0.10‰). Zinc isotope compositions in the studied Ni—Mo sulfide layers, however, have a much wider range (from 0.46‰ to 1.43‰) than their host rocks (Fig. 4B). Moreover, the δ^{66}Zn values of Ni—Mo sulfide layers follow a trend, increasing from the Nayong section (SW) to the Zunyi and Zhangjiajie sections (NE) (Fig. 4B). δ^{66}Zn is inversely correlated with Zn concentration. The lightest δ^{66}Zn values (from 0.46‰ to 0.64‰, average 0.54 ± 0.06‰), detected in the Nayong Ni—Mo sulfide layer are lower than those of host black shales. Heavier δ^{66}Zn values of Ni—Mo sulfide layers in the Zunyi section (from 0.83‰ to 1.10‰, average 1.00 ± 0.11‰) are heavier than those of host black shales. The heaviest δ^{66}Zn values (from 1.19‰ to 1.43‰, average 1.34 ± 0.09‰) observed in the Zhangjiajie section are accompanied by much lighter δ^{66}Zn values in host black shales.

4.2. Authigenic Mo, U concentrations

All black shale samples from the three studied sections show a wide range in Mo (25–328 ppm) and U (9–113 ppm) concentrations (Table 1 and Fig. 5A). For example, Mo and U concentrations vary from 25 ppm to 64 ppm (mean = 45 ppm) and 23 ppm to 35 ppm (mean = 28 ppm) in the Nayong section, respectively. Generally, Mo and U concentrations in the Zunyi and Zhangjiajie sections are higher than those of the Nayong section. Apart from one relatively low value (49 ppm), Mo values in the Zunyi section (188 ppm to 329 ppm) are slightly higher than those in the Zhangjiajie section (116 ppm to 216 ppm). Uranium concentrations vary from 9 ppm to 113 ppm in the Zunyi section and from 33 ppm to 56 ppm in the Zhangjiajie section. The Nayong black shales show relatively low average Mo_{EF} (65 ± 20) and U_{EF} (13 ± 4). The high and wide ranges of Mo_{EF} (198–892) and U_{EF} (7–72) values are typical of the Zunyi and Zhangjiajie sections (Fig. 6).

Three studied Ni—Mo sulfide layers show anomalous Mo and U enrichment, with extremely high Mo_{EF} (mostly >10,000) and U_{EF} (mostly >100) values (Fig. 6). Furthermore, Mo exhibits a regular decreasing trend from the Nayong and the Zunyi section, to the Zhangjiajie section, with average values ranging from 4.7 wt% to 0.9 wt% (Fig. 5B). For example, the Nayong Ni—Mo sulfide layers show the highest Mo values, ranging from 3.0 wt% to 7.3 wt%, but with varied U values from 11 to 520 ppm. The Mo and U values in the Zunyi section are mostly between 3.0 wt% and 6.6 wt% for Mo, and from 149 ppm to 238 ppm for U. The Mo and U concentrations in the Zhangjiajie section vary from 0.2 wt% and 1.8 wt% for Mo, and from 225 ppm to 716 ppm for U.

5. Discussion

5.1. The redox conditions of deposition

Mo_{EF}–U_{EF} co-variation (Fig. 6) can trace paleo-oceanic redox conditions based on differences in the mechanism of authigenic enrichment between Mo and U across the sediment-water interface (Tribovillard et al., 2006, 2012; Algeo and Tribovillard, 2009; Scott and Lyons, 2012). Generally, uranium enrichment occurs under suboxic conditions, near the redox boundary between Fe (III) and Fe (II), via the formation of UO_2, U_3O_7 or U_3O_8 in sediments (e.g., Crusius et al., 1996; Zheng et al., 2000; Chaillou et al., 2002; Partin et al., 2013). However, the enrichment of Mo in sediments requires the conversion of soluble MoO_4^{2-} to particle-reactive thiomolybdates ($MoO_xS_{4-x}^{2-}$) which can be effectively scavenged by metal-rich particles or sulfidized organic materials (e.g., Helz et al., 1996; Erickson and Helz, 2000; Tribovillard et al., 2004). This conversion with the origin of reactive thiomolybdate occurs mainly in the presence of free hydrogen sulfide (H_2S) (Helz et al., 1996). Therefore, extreme enrichment of Mo in comparison to U occurs under euxinic conditions, where Mo and U show strong enrichment (EFs > 10), with Mo_{EF} often greater than U_{EF} values.

In this study, almost all black shales from the Zunyi and Zhangjiajie sections have Mo concentrations >100 ppm and Mo_{EF} values (198–892) higher than U_{EF} values (7–69), which is indicative of dominantly euxinic conditions. This is not only consistent with V/Cr and Ni/Co values reported by Xu et al. (2012) and Pagès et al. (2018), but also supported by Fe speciation data (Xu et al., 2012; Wen et al., 2014, 2015). The lower Mo concentrations (25–64 ppm) in the Nayong section resulted from anoxic or intermittently euxinic conditions and is consistent with conclusions of Han et al. (2015). In addition, $(Mo/U)_{auth}$ ratios of 0.3–1 times of modern seawater suggest anoxic conditions while $(Mo/U)_{auth}$ ratios of 1–3 times of modern seawater indicate euxinic conditions (Algeo and Tribovillard, 2009; Tribovillard et al., 2012). The $(Mo/U)_{auth}$ ratios in our black shales are mostly between 1 and 3 times of modern seawater, even higher than 3 times of modern seawater (Fig. 6), suggesting prevailing euxinic conditions, which is consistent with previous studies (e.g., Pagès et al., 2018). Much higher $(Mo/U)_{auth}$ ratios (>3 times of modern seawater), Mo_{EF} (mostly >10,000) and U_{EF} (mostly >100) values in Ni—Mo sulfide layers in our three sections could be also linked to their origin in dominantly euxinic environment. Such conditions have been indicated by numerous authors who suggested their possible important role in the accumulation of metals in Ni—Mo sulfide layers (e.g., Jiang et al., 2007; Lehmann et al., 2007; Xu et al., 2012; Pagès et al., 2018).

5.2. Zn isotope composition of black shale

Zinc isotope composition of organic-rich sediments commonly record the mixing of mainly sulfide and an organic-complex phase (Little et al., 2016), reflecting Zn isotopic signals of overlaying seawater under euxinic conditions (Vance et al., 2016; Isson et al., 2018). For example, Zn isotopes in modern euxinic organic-rich sediments from the Black Sea (0.6‰) and the Cariaco Basin (0.50 ± 0.07‰) are consistent with that of modern deep seawater (0.50 ± 0.14‰) (Maréchal et al., 2000; Little et al., 2014), depending on a near-quantitative Zn drawdown from overlying seawater (Vance et al., 2016; Isson et al., 2018). Moreover, Isson et al. (2018) suggested that Zn isotopes of dissolved Zn in seawater over geologic time can be approximated by sulfide phase in black shales deposited in ancient anoxic conditions. Our black shales were estimated to precipitate from euxinic and anoxic seawater (Xu et al., 2012; Wen et al., 2014, 2015; Pagès et al., 2018; this study). As such, Zn isotope composition in our black shales from the three different sections could reflect that of overlying seawater. Based on this

Table 1
δ^{66}Zn values and element concentrations of Niutitang Formation black shale and Ni—Mo Sulfide layer from the Nayong, Zunyi and Zhangjiajie region.

Sample	Location	Lithology	Location	δ^{66}Zn	2σ	Zn_{Auth}	S	TOC	Al	Fe	Mo	U	Zn-Total	Mo_{EF}	U_{EF}	Fe_{HR}/Fe_T	Fe_{PY}/Fe_{HR}
			m	‰		ppm	%	%	%	%	ppm	ppm	ppm				
Zhangjiajie section (N 29°11′, E 110°54′)																	
ZJJ-3	Zhangjiajie	Upper black shale	1.5	0.57	0.07	125	4.53	7.47	3.82	2.91	118	33.2	167	309	28	0.69	0.87
ZJJ-4	Zhangjiajie	Upper black shale	1	0.68	0.07	157	3.38	7.14	3.55	2.84	132	48.6	242	373	44	0.49	0.83
ZJJ-5	Zhangjiajie	Upper black shale	0.5	0.55	0.01	134	4.85	8.13	3.88	2.97	139	48.1	217	359	40	0.43	0.80
	Duplicate			*0.47*	*0.01*	*133*											
	Average			**0.51**		**133**											
ZJJ-6	Zhangjiajie	Ni-Mo-Zn sulfide layer	0	1.43	0.01	6273	14.86	3.95	1.01	6.37	18,381	716	6760	182,918	2298		
	Duplicate			*1.38*	*0.03*	*6590*											
	Average			**1.41**		**6432**											
ZJJ-8	Zhangjiajie	Ni-Mo-Zn sulfide layer	0	1.19	0.03	931	7.07	6.93	2.45	3.33	2740	225	1390	11,214	297		
	Duplicate			*1.23*	*0.07*	*943*											
	Average			**1.21**		**937**											
ZJJ-9	Zhangjiajie	Ni-Mo-Zn sulfide layer	0	1.40	0.01	3009	9.46	3.04	0.50	3.37	15,960	551	2880	321,030	3575		
	Duplicate			*1.35*	*0.07*	*3076*											
	Average			**1.38**		**3043**											
ZJJ-11	Zhangjiajie	Ni-Mo-Zn sulfide layer	0	1.41	0.01	2519	10.07	3.18	0.55	3.49	17,831	546	2690	327,325	3233		
ZJJ-20	Zhangjiajie	Lower black shale	0.2	0.56	0.02	129	3.84	6.34	2.59	2.59	116	55.7	175	449	69		
ZJJ-24	Zhangjiajie	Lower black shale	0.6	0.77	0.06	181	3.39	8.52	2.42	2.20	216	54	218	892	72	0.95	0.73
Zunyi section (N 27°41′, E 106°40′)																	
KXZ-07	Zunyi	Upper black shale	2.5	0.71	0.04	348	3.85	7.37	8.02	4.86	188	20.7	348	235	8	0.59	0.87
KXZ-06	Zunyi	Upper black shale	2	0.82	0.07	553	4.72	9.60	7.96	5.79	271	71.1	553	341	29	0.62	0.87
KXZ-05	Zunyi	Upper black shale	1.7	0.77	0.05	771	4.22	11.25	7.50	6.13	328	112.9	771	438	49	0.59	0.89
	Duplicate			*0.76*	*0.07*	*762*											
	Average			**0.77**		**766**											
KXZ-Ni—Mo	Zunyi	Ni-Mo-Zn sulfide layer	0	0.83	0.01	1820	18.50	9.38	1.24	9.87	46,100	149	1600	370,914	387		
	Duplicate			*0.91*	*0.01*	*1942*											
	Average			**0.87**		**1881**											

(continued on next page)

Table 1 (*continued*)

Sample	Location	Lithology	Location	$\delta^{66}Zn$	2σ	Zn_{Auth}	S	TOC	Al	Fe	Mo	U	Zn-Total	Mo_{EF}	U_{EF}	Fe_{HR}/Fe_T	Fe_{PY}/Fe_{HR}
			m	‰		ppm	%	%	%	%	ppm	ppm	ppm				
XZ-08-01	Zunyi	Ni-Mo-Zn sulfide layer	0	1.09	0.04	2371	12.78	11.10	2.58	8.12	30,030	238	2877	116,353	297		
	Duplicate			*1.10*	*0.04*	*2424*											
	Average			**1.09**		**2398**											
XZ-08-02	Zunyi	Ni-Mo-Zn sulfide layer	0	1.09	0.01	2134	22.51	9.16	1.41	13.34	65,950	171	2614	468,785	392		
KXZ-03	Zunyi	Lower black shale	−0.3	0.89	0.03	172	5.20	7.60	9.41	4.48	188	21	172	200	7	0.66	0.94
KXZ-02	Zunyi	Lower black shale	−0.8	0.76	0.02	115	5.20	7.80	8.98	5.24	314	26.1	115	350	9	0.64	0.93
KXZ-01	Zunyi	Lower black shale	−1.3	0.78	0.02	42	0.78	10.62	2.48	1.97	49	9.2	42	198	12	0.49	0.54
						Nayong section (N 26°44′, E 115°36′)											
6–7	Nayong	Upper black shale	4	0.94	0.03	289		3.04	7.93	3.65	64	26.4	317	81	11		
6–8	Nayong	Upper black shale	2	0.71	0.01	204		3.88	6.01	15.90	48.6	35.4	186	81	19		
JL − 1	Nayong	Ni-Mo-Zn sulfide layer	0	0.61	0.04	128,025		8.37	0.32	13.02	29,857	520	116,712	925,458	5199		
	Duplicate	*Re-powder sample*		*0.48*	*0.04*	*76,923*											
	Average			**0.54**		**102,474**											
3–2	Nayong	Ni-Mo-Zn sulfide layer	0	0.54	0.05	58,313		8.95	0.72	16.10	49,905	354	49,439	693,818	1588		
5–4	Nayong	Ni-Mo-Zn sulfide layer	0	0.64	0.03	147,583		9.74	0.51	12.25	37,492	512	115,515	730,815	3219		
	Duplicate	*Re-powder sample*		*0.46*	*0.04*	*74,510*											
	Average			**0.55**		**111,047**											
6–10	Nayong	Ni-Mo-Zn sulfide layer	0	0.53	0.06	94,365		11.45	0.50	18.69	72,913	11.2	95,774	1,451,182	72		
6–12	Nayong	Lower black shale	-1	0.77	0.09	369		3.72	7.09	3.05	41.9	23	353	59	10		
6–14	Nayong	Lower black shale	−6	0.70	0.01	192		4.26	6.30	2.91	25	26.3	199	40	13		
	Duplicate	*Re-powder sample*		*0.59*	*0.04*	*200*											
	Average			**0.65**		**196**											
NOD-P-1		Manganese nodule		0.81($n = 10$)	0.09	1306					692	4.06	1451				
	Reference value*			**0.87**	**0.09**						**760**		**1600**				
NOD-A-1		Manganese Nodule		0.99($n = 10$)	0.08	498					396	7.26	527				
	Reference value*			**1.05**	**0.09**						**448**		**590**				

Mo, U concentrations and Fe species data in the Zhangjiajie section are from Fan et al. (2012) and Wen et al. (2014).
Mo, U, Zn(total), TOC, Fe, Al and Fe species data in the Zunyi section are from Wen et al. (2015).
Mo, U, Zn(total), and TOC concentrations in the Nayong section are from Han et al. (2015).
* Reference data from Isson et al. (2018).

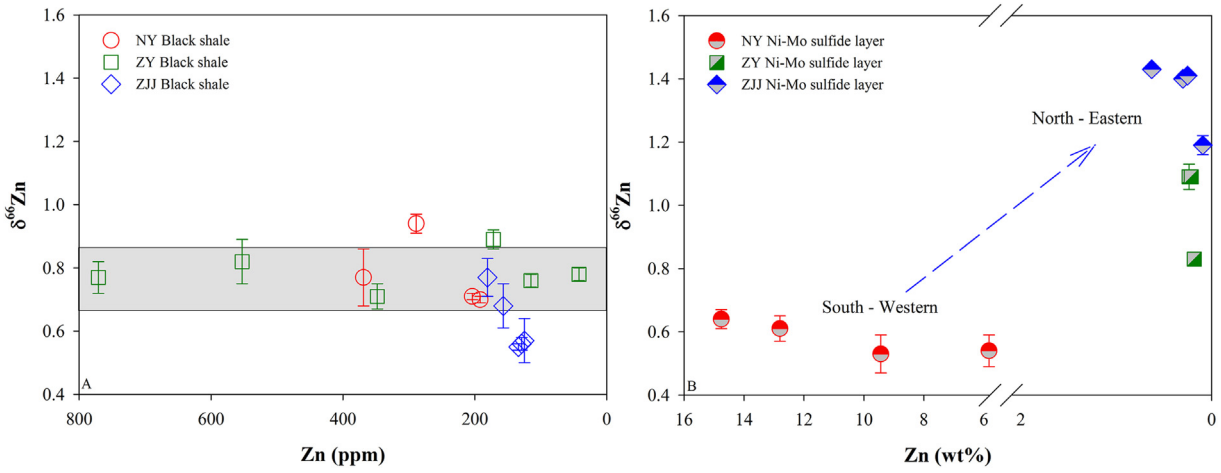

Fig. 4. Zn isotope compositions plotted against Zn concentrations in all black shales (A) and Ni—Mo polymetallic sulfide layers (B). The gray shade area represents the average of δ^{66}Zn values of black shales in the Nayong and Zunyi sections from Guizhou province (A). A regular increasing trend in δ^{66}Zn values of Ni—Mo sulfide layers is observed from the South-Western (SW) Nayong to the North-Eastern (NE) Zhangjiajie, which is marked by a blue arrow (B).

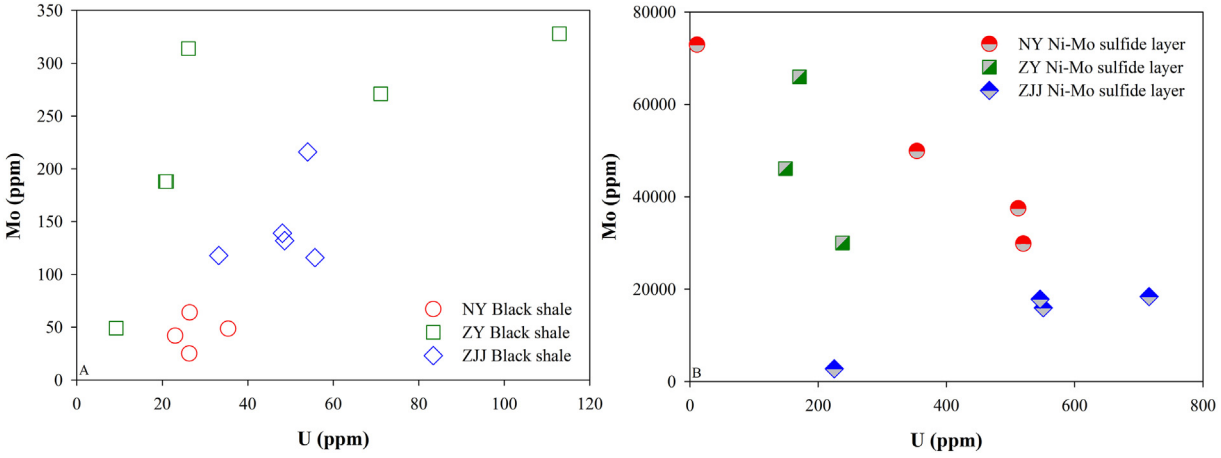

Fig. 5. Mo vs. U concentrations in all black shales (A) and Ni—Mo polymetallic sulfide layers (B). Two reverse trends between Mo and U concentrations are observed in black shales (A) and Ni—Mo polymetallic sulfide layers (B).

assumption, Zn isotope composition of ambient seawater should be close to 0.76 ± 0.09‰ (1σ) at the Nayong and Zunyi sections, and slightly lower at the Zhangjiajie section (0.59 ± 0.10‰, 1σ), which may be associated with different depth of seawater and/or mixing where the proportion of sulfide and organically-bound Zn were different. Alternatively, Ackerman et al. (2019) explained δ^{66}Zn values (0.09 to 0.67‰) in normal and highly metalliferous Neoproterozoic/Cambrian black shales from the Bohemian Massif in terms of variable proportions of high-metal authigenic and low-metal terrigenous sources. They also confirmed that the authigenic δ^{66}Zn value of 0.36 ± 0.16‰ for the highly metalliferous black shales is similar to that of the present-day deep ocean, which implies that the Zn isotopic composition of the ocean remained constant from the Neoproterozoic because of the well-balanced cycle of phosphates (Ackerman et al., 2019).

Previous studies suggested that bioavailable Zn accumulated by phytoplankton along a north-south transect of the Tasman Sea results in light Zn isotopic composition (Samanta et al., 2017), but others indicated that the surface adsorption of organism commonly scavenged isotopically heavy Zn (John and Conway, 2014; Köbberich and Vance, 2017). Most recently, Isson et al. (2018) provided clear evidence of biological transport of isotopically light Zn into the organic-rich sediments. For example, δ^{66}Zn values of organisms (bitumen and kerogen) is 0.36‰–0.26‰ lower than those of sulfide in the same shale samples after ~800 Ma. However, the low Zn concentrations in bitumen

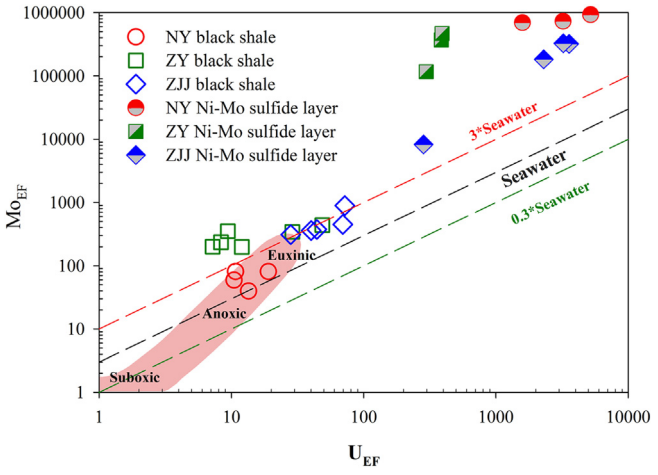

Fig. 6. The co-variations of Mo and U enrichment factors. The pink shadow represent the trend from suboxic, anoxic to euxinic conditions following Algeo and Tribovillard (2009). The average Mo/U weight ratio of seawater is 3.1 (the Mo/U molar ratio is 7.5–7.9, Algeo and Tribovillard, 2009; Tribovillard et al., 2012).

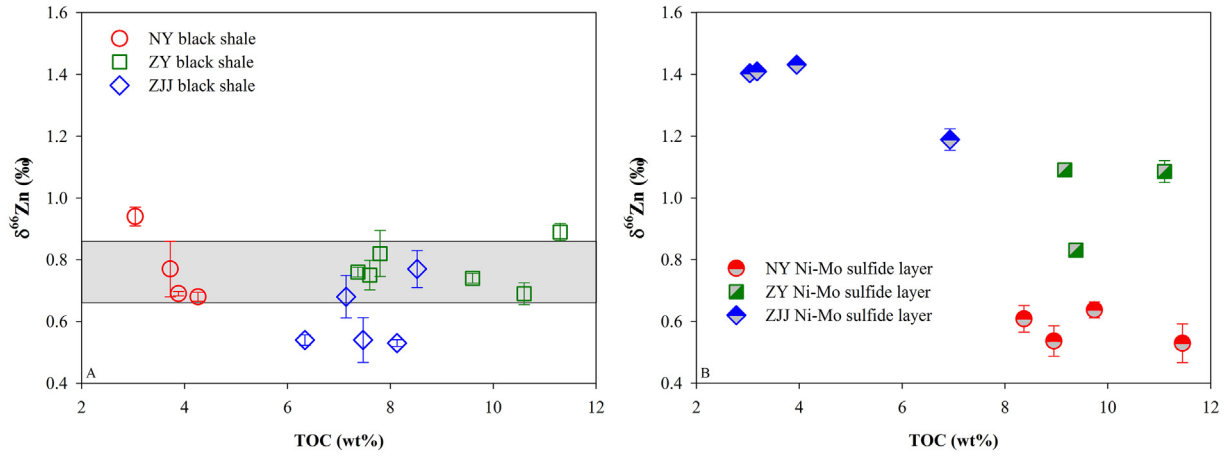

Fig. 7. The relationship between δ^{66}Zn values and total organic carbon (TOC) concentrations in all host black shales (A) and Ni—Mo polymetallic sulfide layers (B) in three investigated sections. The gray shade area (A) represents the average of δ^{66}Zn values of black shales in the Nayong and Zunyi sections from Guizhou province.

(Steiner et al., 2001) and the absence of a relationship between δ^{66}Zn values and TOC ratios in our investigated shales (Fig. 7A), indicate that the admixture of organism-derived Zn in large proportion is not the primary driver of lighter Zn isotopic composition in the Zhangjiajie section.

The Zn isotope composition of modern seawater varies with depth: shallow water shows a high degree of spatial variability in δ^{66}Zn values (from −1.0‰ to 1.0‰; Conway and John, 2014), but δ^{66}Zn value is homogenous at depth (~0.50 ± 0.14‰, Maréchal et al., 2000; Little et al., 2014). The paleogeography of the Zhangjiajie area indicates a slope location (Chen et al., 2009). The δ^{66}Zn values of the Zhangjiajie section is similar to or slightly higher than that of modern deep seawater, which might indicate that deep seawater in the Nanhua Basin may have been similar to modern deep-water Zn isotope composition during early Cambrian. Previous studies also indicate δ^{66}Zn values for deep seawater of the Nanhua Basin near 0.5‰ during early Ediacaran, based on relatively homogenous Zn isotope compositions in slope and basin organic-rich shales deposited under euxinic conditions (0.45‰, Fan et al., 2018; 0.52‰, Isson et al., 2018). However, the slightly higher δ^{66}Zn values (0.76 ± 0.09‰) of the water column in the Nayong and Zunyi sections are very similar to the variation in modern intermediate depth seawater. For example, δ^{66}Zn values at depth of a few hundred meters from the northeastern Atlantic and Southern Ocean (Atlantic sector) exhibit a positive excursion of up to 0.7‰ (Conway and John, 2014, 2015; Zhao et al., 2014). These observations from different modern oceans reported by different researchers indicate that Zn isotopic fractionation associated with internal cycling resulted from the regeneration of isotopically heavy Zn adsorbed onto organisms and Fe—Mn oxides or the precipitation of isotopically light Zn in sulfides (Conway and John, 2014, 2015; John and Conway, 2014; Zhao et al., 2014).

As mentioned above, δ^{66}Zn values of the Nayong and Zunyi shales recorded ambient seawater signals. Therefore, it is also possible that the seawater of the Nanhua Basin has a positive excursion at the intermediate depth. A stratified redox ocean model (Li et al., 2017) might help to explain the slightly heavier Zn isotope composition in the Nanyong and Zunyi sections when compared to modern deep water. In shallow oxic water, Fe—Mn oxides and hydroxides preferentially absorb heavy Zn from the water column (Δ^{66}Zn ~ 0.3–0.5‰, Pokrovsky et al., 2005; Gélabert et al., 2006; Jouvin et al., 2009). Along with the precipitation of Fe oxides, the isotopically heavy Zn adsorbed on the surface of Fe-oxides would be released into the water column again accompanied with the reduction of Fe oxides. In euxinic conditions, these heavy Zn isotopes would be preserved in anoxic sediments. Meanwhile, phytoplankton could uptake isotopically light Zn (Samanta et al., 2017) and organic particles with isotopically heavy Zn (Gélabert et al., 2006; John et al., 2007; John and Conway, 2014). Even though organisms transport isotopically light Zn into the organic-rich sediments (Isson et al., 2018), Zn isotopic composition in our black shales most likely reflects that of sulfide phase, given the lower Zn concentrations in bitumen.

In summary, our organic-rich shales deposited in a euxinic/anoxic environment captured the Zn isotope composition of ambient seawater. The δ^{66}Zn values of the Zhangjiajie shales are very close to those of modern deep seawater. On the other hand, δ^{66}Zn values of the Nayong and Zunyi shales most likely reflect Zn isotope fractionation during Fe—Mn oxide shuttling processes in a stratified redox ocean.

5.3. Large variation of Zn isotopes in Ni—Mo sulfide layers

Three investigated Ni—Mo sulfide layers show a wide range in Zn isotope compositions (from 0.46‰ to 1.43‰). Moreover, δ^{66}Zn values show a striking trend in our studied Ni—Mo polymetallic sulfide layers, increasing from SW to NE (Fig. 4B). Previous studies suggested that Ni—Mo sulfide layers have been deposited under dominantly euxinic conditions (Pagès et al., 2018). Therefore, Ni—Mo sulfide layers should preserve the same δ^{66}Zn values as host black shales, if seawater was a major Zn source. However, δ^{66}Zn values in these sulfide layers differ significantly from those of their host black shales. For example, the average δ^{66}Zn value (0.54 ± 0.09‰) in sulfide layer from the Nayong section is 0.2‰ lower than that of host black shales (0.73 ± 0.12‰). The average δ^{66}Zn value (1.34 ± 0.09‰) in sulfide layer from Zhangjiajie section is much higher than that of host black shales (0.59 ± 0.10‰). There are two possible mechanisms to explain such a large variation of Zn isotope composition in these sulfide layers: 1) the mixing of different proportions of organism and sulfide phase, 2) important inputs of other metal sources, such as continental weathering and/or hydrothermal fluids.

Previous studies suggested that organic matter could play important roles in transporting and precipitating metals into Ni—Mo sulfide layers (e.g., Coveney Jr. and Pašava, 2004; Kříbek et al., 2007; Orberger et al., 2007; Cao et al., 2013; Lehmann et al., 2016). Recent studies proposed that organisms can export light Zn isotope into sediments, δ^{66}Zn values in euxinic sediments would approach that derived from organisms if biological uptake is the main process (Isson et al., 2018). This mechanism is likely a potential control for higher δ^{66}Zn values in the Zhangjiajie sulfide layers and lower values in the Nayong section. The broadly negative correlation between δ^{66}Zn values and TOC concentrations for sulfide layers in the three locations ($R^2 = 0.62$, Fig. 7B) might indicate that the mixing proportion of organisms in the Nayong and Zunyi sections was high. However, the following four observations don't support this interpretation. Firstly, Zn concentrations do not show a positive

correlation with TOC. Secondly, the Nayong and Zunyi sulfide layers contain similarly high TOC content, but with a large difference of $\delta^{66}Zn$ value. Thirdly, the average $\delta^{66}Zn$ difference between sulfide layer and black shale values in the Zhangjiajie section reaches up to ~0.9‰, which is two times higher than $\Delta^{66}Zn_{organism\text{-}seawater}$ ~ 0.36‰ post 800 Ma reported by Isson et al. (2018). Finally, Zn concentrations (several weight percent) in the Nayong sulfide layer are much higher than those in samples controlled by biological uptake, although the average $\delta^{66}Zn$ difference between sulfide layer and black shale is similar to $\Delta^{66}Zn_{organism\text{-}seawater}$ ~ 0.36‰ published by Isson et al. (2018). Therefore, we argue that biological processes could not have played a major role in producing the large variation of Zn isotope compositions in our investigated sulfide layers.

As already mentioned, Zn is commonly present as sphalerite in association with Ni-sulfide minerals (Fig. 3). Based on the different Ni isotope compositions of sulfide layers (−0.84 ± 0.09‰) and host black shales (mostly near 0.08 ± 0.14‰), Pašava et al. (2018) suggested that Ni in sulfide layers from the Zunyi section did not originate from ambient seawater but was instead derived from continental weathering of ultra-mafic and mafic-rock. During precipitation, organic matter played an important role in the accumulation of Ni and Mo (Kříbek et al., 2007; Orberger et al., 2007; Cao et al., 2013). Zn isotopes, however, do not support such a source, because weathering of ultra-mafic and mafic rocks commonly produces a minor Zn isotope fractionation (<0.2‰, Lv et al., 2016; Suhr et al., 2018), and it would be impossible to elevate Zn isotopic values close to 1.4‰.

Alternatively, hydrothermal contribution could be another possible control inducing large and regular variations of Zn isotopes. For example, Wilkinson et al. (2005) first observed systematically increasing in $\delta^{66}Zn$ in sphalerites from different ore-forming stages in the Irish ore field, including source-closed feeder veins (−0.17 ± 0.17‰–0.04 ± 0.02‰), orebodies-closed feeder veins (0.02 ± 0.05‰–0.16 ± 0.13‰), major orebodies (0.28 ± 0.10‰–1.33 ± 0.24‰). The same trends have also been reported from the Sichuan-Yunnan-Guizhou Pb—Zn Metalliferous region in South China (Zhou et al., 2014). Similarly, different deposits in a large Red Dog polymetallic district (USA) also exhibit systematically increasing in $\delta^{66}Zn$ values northward (Kelley et al., 2009), namely from the Main (0.13‰–0.25‰) and Aqqaluk deposits (0.01‰–0.3‰) to the Paalaaq deposit (0.24‰–0.25‰), with the heaviest Zn isotope values (0.39‰–0.60‰) at the Anarraaq deposit. These observations could reflect Zn isotope Rayleigh fractionation during the regional ore-forming fluid migrating processes. The three investigated Ni—Mo sulfide layers have been found to originate almost simultaneously (~521 ± 5 Ma, Xu et al., 2011; ~526.5 ± 5.6 Ma, Lan et al., 2017). They are distributed from SW to NE along the southern paleo-continental margin of the Yangtze Platform (Steiner et al., 2001; Mao et al., 2002) and the distribution of Ni—Mo sulfide layers is consistent with the possible SW–NE striking large deep faults (Steiner et al., 2001). Moreover, the Zn isotopic composition of these Ni—Mo sulfide layers is similar to previously observed trends in the Red Dog district (Kelley et al., 2009), which might indicate active involvement of hydrothermal fluids during Zn enrichment. During the fluid migration along the belt from SW to NE at the southern margin of the Yangtze Platform, the isotopically light Zn would dominate at the near-source Nayong location, and then heavier Zn isotope would participate in the deposition of Ni—Mo sulfide layer in Zunyi, and the heaviest Zn isotopes would be trapped in the most remote Zhangjiajie region.

If this was true, these three sulfide layers could represent different development stages of fluid migration, during which the precipitated portion of Zn initially dissolved in hydrothermal fluid can be estimated using a Rayleigh fractionation model. $\delta^{66}Zn_{Ni\text{-}Mo} = \delta^{66}Zn_{HY} + \varepsilon^*(1 + \ln(f))$, where $\delta^{66}Zn_{Ni\text{-}Mo}$ is the Zn isotope composition of sulfide layer; $\delta^{66}Zn_{HY}$ is the initial Zn isotope composition of hydrothermal fluids (0.27‰, Mason et al., 2005); f is the fraction of dissolved Zn remaining in the hydrothermal fluid, and ε is Zn isotope fractionation between hydrothermal fluid and sulfide layer (−0.36‰, e.g., Fujii et al., 2011; Veeramani et al., 2015; Jamieson-Hanes et al., 2017). According to Fig. 8, the lowest $\delta^{66}Zn$ values correspond to about 82% of dissolved Zn having been precipitated from hydrothermal fluid before arriving at the Nayong location. The most positive $\delta^{66}Zn$ values at Zhangjiajie can be achieved after precipitation of ~97% dissolved Zn from hydrothermal fluids. This can also explain a previous observation (Lan et al., 2017) where Ni—Mo sulfide layer from Yichang (North of Zhangjiajie) in Hubei province contains similarly low Zn concentrations (~481 ppm) as the host black shales.

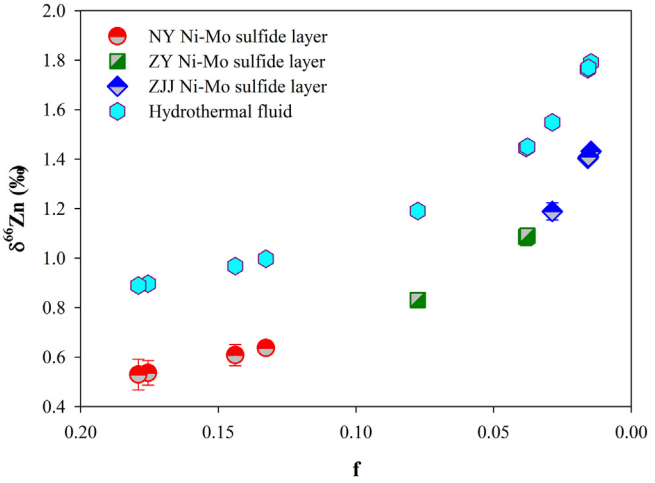

Fig. 8. Rayleigh fractionation of Zn isotope during the migration of hydrothermal fluids. f is the fraction of dissolved Zn remaining in the hydrothermal fluid. The hydrothermal fluid could be associated with Pb—Zn mineralization event, with the initial Zn isotope composition of ~0.27‰.

In short, Zn isotope compositions in Ni—Mo sulfide layers are not consistent with their seawater signature. We suggest that large variations of Zn isotopes could result from Rayleigh fractionation during hydrothermal fluid migrating from the Nayong (SW) to Zhangjiajie (NE).

5.4. Implications for Zn source in Ni—Mo sulfide layers

After forty years of debate, the latest studies on Ni—Mo sulfide layers have not reached consensus about different sources of metals (see Introduction in this paper for more details).

Here, we discuss possible metal Zn sources in these sulfide layers. In general, the highest Zn concentrations reported from this type of mineralization were described from the Nayong section in Guizhou province (11 wt%, Han et al., 2015) and Deze in Yunnan province (3 wt%, Chen et al., 1982). Lower Zn enrichments (~thousands ppm) were reported from Zunyi and Zhangjiajie (Xu et al., 2012; Han et al., 2015; this study), while the lowest Zn concentrations (several hundred ppm) were found at Yichang in Hubei province (Lan et al., 2017). This regional distribution of Zn enrichment could be associated with local metallogenic events. The Pb—Zn mineralization hosted in the Neoproterozoic dolostone of the Dengying Formation at the border of Sichuan, Yunnan and Guizhou provinces, accounts for ~50% of Zn + Pb ore deposits in this metallogenic province (Shao and Li, 1996), and some of them may have a similar and/or slightly later mineralization age compared to the Ni—Mo sulfide layer (needs further investigation). These Pb—Zn metallogenic events may have provided abundant metal Zn for the formation of sulfide layers at the Nayong and Deze locations. In addition, the Dujiaqiao Pb—Zn deposit hosted in the Dengying Formation dolostone is located only 30 km south of the Nayong section (Tan et al., 2012). During mineralization processes, >80% dissolved Zn in hydrothermal fluids could precipitate and form Pb—Zn ore deposit. The late stage hydrothermal fluids with low Zn concentrations and higher $\delta^{66}Zn$ values, could continue to migrate along major faults, and

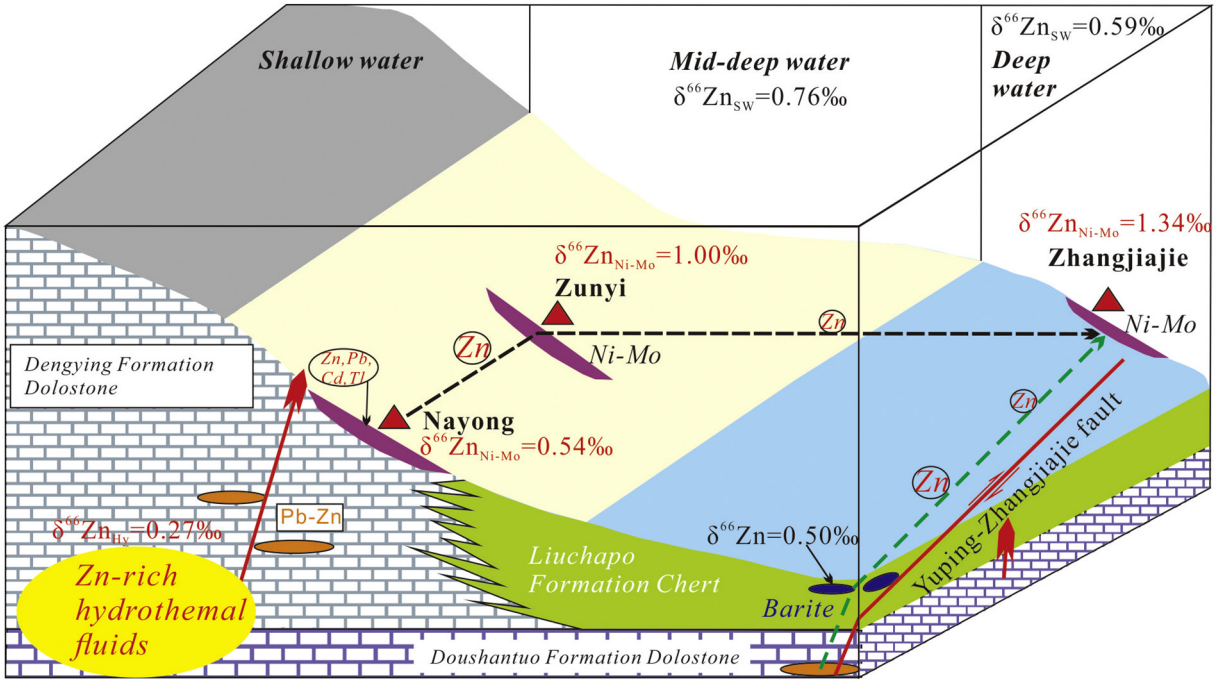

Fig. 9. A cartoon diagram for Zn source in Ni—Mo polymetallic sulfide layers. At the Nayong and Zunyi locations, Zn isotope composition of mid-deep seawater ($\delta^{66}Zn_{SW}$) is ~0.76‰. At the Zhangjiajie location, $\delta^{66}Zn_{SW}$ value of deep water is ~0.59‰. All Ni—Mo sulfide layers did not capture Zn isotope composition of their seawater. Local Pb—Zn metallogenic events could have provided an important source of Zn for Ni—Mo sulfide layer in the Nayong section. Zn isotope fractionation during the migration of hydrothermal fluids resulted in heavier Zn isotope composition at the Zunyi and Zhangjiajie sections (black dash line). Alternatively, near south-north fault (Yuping-Zhangjiajie fault) could have been another possible Zn source for the Zhangjiajie section (shown by a green dash line). The hydrothermal fluids did not altered the black shale sequence or became a source of Mo and Ni in these sulfide layers, but only resulted in different magnitude Zn (Pb, Cd, Tl)-enrichment by overprinting multiple-sourced synsedimentary Ni—Mo sulfide units.

get precipitated at Nayong ($\delta^{66}Zn = 0.54‰$). The lower Zn concentrations and higher $\delta^{66}Zn$ values (1.00‰) at the Zunyi section could reflect a restricted role of hydrothermal activity associated with Pb—Zn metallogenic events (Fig. 9). This interpretation is also consistent with the decreasing enrichment of Pb from1.2 wt% in Zhijin (near Nayong) to 510 ppm in Zunyi (Steiner et al., 2001).

Given the location of the Zhangjiajie section (~500 km away from the Nayong section), another possible Zn source could be considered (Fig. 9). Wen et al. (2017) suggested that there was a large-scale hydrothermal activity in the Nanhua Basin during early Cambrian. The hydrothermal activity could not only have provided an important metal source for Pb—Zn mineralization hosted in the Doushantuo Formation, but also for barite ore deposits hosted in the Liuchapo Formation in the western part of Hunan and eastern part of Guizhou province (Zhou et al., 2018, Zhou, 2018). There are also numerous Pb—Zn ore deposits along the Yuping-Zhangjiajie fault, which is hosted in dolostone of the Doushantuo Formation (Duan, 2014). The available Zn isotope data demonstrate that $\delta^{66}Zn$ values are lower than 0.03‰ in the Dilu Pb—Zn deposit and −0.19‰ in the Dongjiahe Pb—Zn deposit (Zhou, 2018). In contrast, sulfides in the barite ore deposit at the base of the Niutitang Formation have a $\delta^{66}Zn$ of 0.50‰ (Zhou, 2018). The similar trend to the Nayong area might also indicate involvement of hydrothermal activity. We demonstrated that ~97% of dissolved Zn in hydrothermal fluid had been already precipitated before arriving at the Zhangjiajie section (Fig. 8). Therefore, we believe that these Pb—Zn metalogenic events could have provided only minor Zn for sulfide layer in the Zhangjiajie section, but strongly fractionated $\delta^{66}Zn$ values of sulfide layer (Fig. 9). Here, we propose that Zn in these sulfide layers could have been derived from hydrothermal fluids associated with local Pb—Zn metalogenic events.

As mentioned earlier, Ni—Mo polymetallic sulfide layers have been considered to be of sedimentary exhalative (SEDEX) origin, where hydrothermal fluids (basinal brines) leaching the basement and thick carbonate unit, contributed Ni, Mo and Zn to sulfide layers (e.g., Murowchick et al., 1994; Coveney Jr. et al., 1994; Coveney Jr., 2003; Lott et al., 1999). Steiner et al. (2001) proposed that the basal shales were also more or less altered by Ni, Mo, Zn-rich hydrothermal fluids related to volcanics, while the shales overlying the ore layers remained unaffected. Uniformity in $\delta^{66}Zn$ values of host shales demonstrate that Zn-rich hydrothermal fluids associated with Pb—Zn metalogenic events did not affect the whole black shale sequence, but possibly only the black shale very near the sulfide layer. Although hydrothermal fluids related to MVT-type mineralization can leach Mo, Ni and other metals from country rocks (Coveney Jr., 2003, references therein), we do not see any evidence for increased Mo and/or Ni concentrations in these fluids. Therefore, a possible model is that a sulfide-rich unit with multiple sourced synsedimentary Ni-Mo-polymetallic enrichment has been overprinted by Zn-rich hydrothermal fluids associated with MVT-type mineralization (Fig. 9). This hydrothermal overprint event could also result in the hyper-enrichments of some dispersed elements (Cd, Tl, etc.), given their high concentrations in MVT-type Pb—Zn mineralization (Zhou, 2010 and references therein).

6. Conclusions

In this contribution, we report the first Zn isotope data from Ni—Mo polymetallic sulfide layers and their host black shales in the lower Cambrian (south China). The euxinic/anoxic seawater condition resulted in the near-quantitative scavenging of Zn from anoxic/euxinic seawater into the black organic-rich shales, resulting in preservation of seawater $\delta^{66}Zn$ values in these sediments. The $\delta^{66}Zn$ values (average 0.59 ± 0.10‰) in the Zhangjiajie shales indicate that Zn isotope composition of deep-seawater in the Nanhua Basin during the early Cambrian may have been very close to that of modern deep seawater. A slightly higher average $\delta^{66}Zn$ value (0.76 ± 0.09‰) in the Nayong and Zunyi sections could reflect the transport of isotopically heavy Zn during Fe—Mn

oxide shuttle in a stratified redox basin. In contrast, the average δ^{66}Zn values (0.54 ± 0.06‰) in the Nayong Ni—Mo polymetallic sulfide layer is 0.2‰ lower than that of host black shales, but is 0.3–0.7‰ higher in the Zunyi (average 1.00 ± 0.11‰) and Zhangjiajie (average 1.34 ± 0.09‰) sections than host black shales, indicating that none of the studied Ni—Mo polymetallic sulfide layers inherited Zn isotope signal of the ambient seawater. Moreover, the regularly increasing trend in δ^{66}Zn values from Nayong to Zunyi to Zhangjiajie might reflect Rayleigh fractionation of Zn isotopes during the migration of hydrothermal fluids. We suggest that these hydrothermal fluids (a dominant source of Zn) could be associated with the origin of local MVT-type Pb—Zn mineralization hosted in the Dengying/Doushantuo Formation.

CRediT authorship contribution statement

Haifeng Fan: Conceptualization, Methodology, Writing - original draft.**Hongjie Zhang:**Investigation.**Chaoyi Xiao:**Investigation.**Jan Pašava:**Conceptualization, Writing - review & editing.**Tao Han:**Investigation.**Ting Zhou:**Resources.**Hanjie Wen:**Resources.

Acknowledgement

This project was funded by the Strategic Priority Research Program (B) of the Chinese Academy of Sciences (XDB18030302), the National Key Research and Development Program of China (2017YFC0602503), NSFC (U1812402, 41890840, 41573011), CAS IIT (JCTD-2019-17), and Guizhou Science and Technology Foundation ([2010]2029). It is also a contribution to the Research Grant no. 17-15700S of the Czech Grant Agency awarded to Jan Pašava and the Strategic Research Plan of the Czech Geological Survey (DKRVO/ČGS 2018-2022). We thank John M. Hora (Czech Geological Survey) for language improvement. Two anonymous reviewers and Editor are gratefully acknowledged for their suggestions.

Declaration of competing interests

The authors declare that they have no known competing financial interests or personal relationships that could have appeared to influence the work reported in this paper.

References

Ackerman, L., Pašava, J., Šípková, A., Martínková, E., Haluzová, E., Rodovská, Z., Chrastný, V., 2019. Copper, zinc, chromium and osmium isotopic compositions of the Teplá-Barrandian unit black shales and implications for the composition and oxygenation of the Neoproterozoic-Cambrian Sea. Chem. Geol. 521, 59–75.

Algeo, T.J., Tribovillard, N., 2009. Environmental analysis of paleoceanographic systems based on molybdenum–uranium covariation. Chem. Geol. 268, 211–225.

Cao, J., Hu, K., Zhou, J., Shi, C.H., Bian, L.Z., Yao, S.P., 2013. Organic clots and their differential accumulation of Ni and Mo within early Cambrian black-shale-hosted polymetallic Ni–Mo deposits, Zunyi, South China. J. Asian Earth Sci. 62, 531–536.

Chaillou, G., Anschutz, P., Lavaux, G., Schäfer, J., Blanc, G., 2002. The distribution of Mo, U, and Cd in relation to major redox species in muddy sediments of the Bay of Biscay. Mar. Chem. 80, 41–59.

Chen, N.S., Yang, X.Z., Liu, D.H., Xiao, X.J., Fan, D.L., Wang, L.F., 1982. Lower Cambrian black argillaceous and arenaceous rock series in South China and its associated stratiform deposits. Mineral. Deposita 2, 39–51 (In Chinese with English abstract).

Chen, D., Wang, J., Qing, H., Yan, D., Li, R., 2009. Hydrothermal venting activities in the early Cambrian, South China: petrological, geochronological and stable isotopic constraints. Chem. Geol. 258, 168–181.

Conway, T.M., John, S.G., 2014. The biogeochemical cycling of zinc and zinc isotopes in the North Atlantic Ocean. Glob. Biogeochem. Cycles 28. https://doi.org/10.1002/2014GB004862.

Conway, T.M., John, S.G., 2015. The cycling of iron, zinc and cadmium in the North East Pacific Ocean—insights from stable isotopes. Geochim. Cosmochim. Acta 164, 262–283.

Coveney Jr., R.M., 2003. Re-Os dating of polymetallic Ni-Mo-PGE-Au mineralization in Lower Cambrian black shales of South China and its geological significance — a discussion. Econ. Geol. 98, 661–665.

Coveney Jr., R.M., Chen, N.S., 1991. Ni–Mo–PGE–Au-rich ores in Chinese black shales and speculations on possible analogues in the United States. Mineral. Deposita 26, 83–88.

Coveney Jr., R.M., Pašava, J., 2004. Diverse connections between ores and organic matter. Ore Geol. Rev. 24, 1–5.

Coveney Jr., R.M., Murowchick, J.B., Grauch, R.I., Glascock, M.D., Denison, R.J., 1992. Gold and platinum in shales with evidence against extraterrestrial sources of metals. Chem. Geol. 99, 101–114.

Coveney Jr., R.M., Grauch, R.I., Murowchik, J.B., 1994. Metals, phosphate and stone coal in the Proterozoic and Cambrian of China; the geologic setting of precious metal-bearing Ni–Mo ore beds. Soc. Explor. Geophys. Newsl. 18, 1–11.

Crusius, J., Calvert, S., Pedersen, T., Sage, D., 1996. Rhenium and molybdenum enrichments in sediments as indicators of oxic, suboxic, and sulfidic conditions of deposition. Earth Planet. Sci. Lett. 145, 65–78.

Distler, V.V., Yudovskaya, M.A., Mitrofanov, G.L., Prokof'ev, V.Y., Lishnevskii, E.N., 2004. Geology, composition, and genesis of the Sukhoi Log noble metals deposit, Russia. Ore Geol. Rev. 24, 7–44.

Duan, Q.F., 2014. The Research of the Metallogenic Regularity of Stratabound Zina-Lead Deposits from Sinian-Cambrian in the Western Hunan and Eastern Hubei Ph.D. Thesis, Wuhan (In Chinese with English abstract).

Erickson, B.E., Helz, G.R., 2000. Molybdenum (VI) speciation in sulfidic waters: stability and lability of thiomolybdates. Geochim. Cosmochim. Acta 64, 1149–1158.

Fan, D.L., 1983. Polyelements in the Lower Cambrian black shale series in southern China. In: Augustithis, S.S. (Ed.), The Significance of Trace Elements in Solving Petrogenetic Problems and Controversies. Theophrastus Publications S. A., Athens, pp. 447–474.

Fan, D.L., Yang, R.Y., Huang, Z.X., 1984. The Lower Cambrian Black Shale Series and Iridium Anomaly in South China. Developments in Geoscience, 27th International Geological Congress. Beijing Science Press, Moscow, pp. 215–224.

Fan, H.F., Wen, H.J., Hu, R.Z., Zhao, H., 2011. Selenium speciation in lower Cambrian Se-enriched strata in South China and its geological implications. Geochim. Cosmochim. Acta 75, 7725–7740.

Fan, H., Wen, H., Zhang, Y.X., Zhu, C.W., Huang, J., Chu, X.L., 2012. The S and Se isotope of Lower Cambrian Ni-Mo polymetallic layer in South China. Earth Sci. Front. 19, 266–275 (In Chinese with English abstract).

Fan, H.F., Wen, H.J., Zhu, X.K., Hu, R.Z., Tian, S.H., 2013. Hydrothermal activity during Ediacaran-Cambrian transition: silicon isotopic evidence. Precambrian Res. 224, 23–35.

Fan, H., Wen, H., Xiao, C., Zhou, T., Cloquet, C., Zhu, X., 2018. Zinc geochemical cycling in a phosphorus-rich ocean during the early Ediacaran. J. Geophys. Res. C Oceans Atmos. 123, 5248–5260.

Fujii, T., Moynier, F., Pons, M.-L., Albarede, F., 2011. The origin of Zn isotope fractionation in sulfides. Geochim. Cosmochim. Acta 75, 7632–7643.

Gagnevin, D., Boyce, A.J., Barrie, C.D., Menuge, J.F., Blakeman, R.J., 2012. Zn, Fe and S isotope fractionation in a large hydrothermal system. Geochim. Cosmochim. Acta 88, 183–198.

Gélabert, A., Pokrovsky, O.S., Viers, J., Schott, J., Boudou, A., Feurtet–Mazel, A., 2006. Interaction between zinc and freshwater and marine diatom species: surface complexation and Zn isotope fractionation. Geochim. Cosmochim. Acta 70, 839–857.

Han, S.C., Hu, K., Cao, J., Pan, J.Y., Liu, Y., Bian, L.Z., Shi, C.H., 2014. Mineralogy of early Cambrian Ni-Mo polymetallic black shale at the Sancha Deposit, South China: implications for ore genesis. Resour. Geol. 65, 1–12.

Han, T., Zhu, X.Q., Li, K., Jiang, L., Zhao, C.H., Wang, Z.G., 2015. Metal sources for the polymetallic Ni–Mo–PGE mineralization in the black shales of the Lower Cambrian Niutitang Formation, South China. Ore Geol. Rev. 67, 158–169.

Helz, G.R., Miller, C.V., Charnock, J.M., Mosselmans, J.L.W., Pattrick, R.A.D., Garner, C.D., Vaughan, D.J., 1996. Mechanisms of molybdenum removal from the sea and its concentration in black shales: EXAFS evidences. Geochim. Cosmochim. Acta 60, 3631–3642.

Isson, T.T., Love, G.D., Dupont, C.L., Reinhard, C.T., Zumberge, A.J., Dan, A., et al., 2018. Tracking the rise of eukaryotes to ecological dominance with zinc isotopes. Geobiology 16, 341–352.

Jamieson-Hanes, J.H., Shrimpton, H.K., Veeramani, H., Ptacek, C.J., Lanzirotti, A., Newville, M., Blowes, D.W., 2017. Evaluating zinc isotope fractionation under sulfate reducing conditions using a flow-through cell and in situ XAS analysis. Geochim. Cosmochim. Acta 203, 1–14.

Jiang, S.Y., Chen, Y.Q., Ling, H.F., Yang, J.H., Feng, H.Z., Ni, P., 2006. Trace- and rare-earth element geochemistry and Pb–Pb dating of black shales and intercalated Ni–Mo–PGE–Au sulfide ores in Lower Cambrian strata, Yangtze Platform, South China. Mineral. Deposita 41, 453–467.

Jiang, S.Y., Yang, J.H., Ling, H.F., Chen, Y.Q., Feng, H.Z., Zhao, K.D., Ni, P., 2007. Extreme enrichment of polymetallic Ni–Mo–PGE–Au in lower Cambrian black shales of South China: an Os isotope and PGE geochemical investigation. Palaeogeogr. Palaeoclimatol. Palaeoecol. 254, 217–228.

Jiang, S.Y., Pi, D.H., Heubeck, C., Frimmel, H., Liu, Y.P., Deng, H.L., Ling, H.F., Yang, J.H., 2009. Early Cambrian ocean anoxia in South China. Nature 459, E5–E6.

John, S.G., Conway, T.M., 2014. A role for scavenging in the marine biogeochemical cycling of zinc and zinc isotopes. Earth Planet. Sci. Lett. 394, 159–167.

John, S.G., Geis, R.W., Saito, M.A., Boyle, E.A., 2007. Zinc isotope fractionation during high-affinity and low-affinity zinc transport by the marine diatom *Thalassiosira oceanica*. Limnol. Oceanogr. 52, 2710–2714.

John, S.G., Rouxel, O.J., Craddock, P.R., Engwall, A.M., Boyle, E.A., 2008. Zinc stable isotopes in seafloor hydrothermal vent fluids and chimneys. Earth Planet. Sci. Lett. 269, 17–28.

Jouvin, D., Louvat, P., Juillot, F., Maréchal, C.N., Benedetti, M.F., 2009. Zinc isotopic fractionation: why organic matters. Environ. Sci. Technol. 43, 5747–5754.

Kao, L.S., Peacor, D.R., Coveney, J., Zhao, G., Dungey, K.E., Curtis, M.D., Penner-Hahn, J.E., 2001. A C/MoS2 mixed-layer phase (MoSC) occurring in metalliferous black shales from Southern China, and new data on jordisite. Am. Mineral. 86, 852–861.

Kelley, K.D., Wilkinson, J.J., Chapman, J.B., Crowther, H.L., Weiss, D.J., 2009. Zinc isotopes in sphalerite from base metal deposits on the red dog district, northern Alaska. Econ. Geol. 104, 767–773.

Köbberich, M., Vance, D., 2017. Kinetic control on Zn isotope signatures recorded in marine diatoms. Geochim. Cosmochim. Acta 210, 97–113.
Kříbek, B., Sýkorová, I., Pašava, J., Machovič, V., 2007. Organic geochemistry and petrography of barren and Mo-Ni-PGE mineralized marine black shales of the lower Cambrian Niutitang Formation (South China). Int. J. Coal Geol. 72, 240–256.
Lan, Z.W., Li, X.H., Chu, X.L., Tang, G., Yang, S., Yang, H., Liu, H., Jiang, T., Wang, T., 2017. Sims U-Pb zircon ages and Ni-Mo-PGE geochemistry of the lower Cambrian Niutitang formation in South China: constraints on Ni-Mo-PGE mineralization and stratigraphic correlations. J. Asian Earth Sci. 137, 141–162.
Lehmann, B., Mao, J.W., Li, S.R., Zhang, G.D., 2003. Re–Os dating of polymetallic Ni–Mo–PGE–Au mineralization in Lower Cambrian black shales of South China and its geological significance — a reply. Econ. Geol. 98, 663–665.
Lehmann, B., Nagler, T.F., Holland, H.D., Wille, M., Mao, J.W., Pan, J.Y., Ma, D.S., Dulski, P., 2007. Highly metalliferous carbonaceous shale and Early Cambrian seawater. Geology 35, 403–406.
Lehmann, B., Frei, R., Xu, L., Mao, J., 2016. Early Cambrian black shale-hosted Mo-Ni and V mineralization on the rifted margin of the Yangtze platform, China: reconnaissance chromium isotope data and a refined metallogenic model. Econ. Geol. 111, 89–103.
Li, C., Jin, C.S., Planavsky, N.J., Algeo, T.J., Cheng, M., Yang, X.L., Zhao, Y.L., Xie, S.C., 2017. Coupled oceanic oxygenation and metazoan diversification during the early–middle Cambrian? Geology 45, 743–746.
Little, S.H., Vance, D., Walker-Brown, C., Landing, W.M., 2014. The oceanic mass balance of copper and zinc isotopes, investigated by analysis of their inputs, and outputs to ferromanganese oxide sediments. Geochim. Cosmochim. Acta 125, 673–693.
Little, S.H., Vance, D., Mcmanus, J., Severmann, S., 2016. Key role of continental margin sediments in the oceanic mass balance of Zn and Zn isotopes. Geology 44, 207–210.
Lott, D.A., Coveney Jr., R.M., Murowchick, J.B., Grauch, R.I., 1999. Sedimentary exhalative nickel–molybdenum ores in South China. Econ. Geol. 94, 1051–1066.
Loukola-Ruskeeniemi, K., Lahtinen, H., 2013. Multiphase evolution in the black-shale hosted Ni–Cu–Zn–Co deposit at Talvivaara, Finland. Ore Geol. Rev. 52, 85–99.
Lv, Y.W., Liu, S.A., Zhu, J.M., Li, S.G., 2016. Copper and zinc isotope fractionation during deposition and weathering of highly metalliferous black shales in Central China. Chem. Geol. 445, 24–35.
Mao, J.W., Lehmann, B., Du, A.D., Zhang, G.D., Ma, D.S., Wang, Y.T., Zeng, M.G., Kerrich, R., 2002. Re–Os dating of polymetallic Ni–Mo–PGE–Au mineralization in lower Cambrian black shales of South China and its geologic significance. Econ. Geol. 97, 1051–1061.
Maréchal, C., Nicolas, E., Douchet, C., Albarède, F., 2000. Abundance of zinc isotopes as a marine biogeochemical tracer. Geochem. Geophys. Geosyst. 1, 1–15.
Mason, T.F.D., Weiss, D.J., Chapman, J.B., Wilkinson, J.J., Tessalina, S.G., Spiro, B., Horstwood, M.S.A., Spratt, J., Coles, B.J., 2005. Zn and Cu isotopic variability in the Alexandrinka volcanic-hosted massive sulfide (VHMS) ore deposit, Urals, Russia. Chem. Geol. 221, 170–187.
Murowchick, J.B., Coveney Jr., R.M., Grauch, R.I., Eldridge, C.S., Shelton, K.L., 1994. Cyclic variations of sulfur isotopes in Cambrian stratabound Ni-Mo-(PGE-Au) ores of Southern China. Geochim. Cosmochim. Acta 58, 1813–1823.
Orberger, B., Pašava, J., Gallien, J.P., Daudin, L., Pinti, D., 2003. Biogenic and abiogenic hydrothermal sulfides: controls of rare metal distribution in black shales (Yukon Territories, Canada). J. Geochem. Explor. 78–79, 559–563.
Orberger, B., Vymazalová, A., Wagner, C., Fialin, M., Gallien, J., Wirth, R., Pašava, J., Montagnac, G., 2007. Biogenic origin of intergrown Mo-sulphide- and carbonaceous matter in Lower Cambrian black shales (Zunyi Formation, Southern China). Chem. Geol. 238, 213–231.
Oszczepalski, S., 1989. Kupferschiefer in southwestern Poland: sedimentary environments, metal zoning, and ore controls. In: Boyle RW, Brown AC, Jefferson GF, Jowett EC, Kirkham RV (eds) Sediment-hosted Stratiform Copper Deposits. Geol. Assoc. Can. Spec. Pap. 36, 571–600.
Pagès, A., Barnes, S., Schmid, S., Coveney, R., Schwark, L., Liu, W., Grice, K., Fan, H., Wen, H., 2018. Geochemical investigation of the lower Cambrian mineralised black shales of South China and the late Devonian Nick deposit, Canada. Ore Geol. Rev. 94, 396–413.
Partin, C.A., Bekker, A., Planavsky, N.J., Scott, C.T., Gill, B.C., Li, C., Podkovyrov, V., Maslov, A., Konhauser, K.O., Lalonde, S.V., Love, G.D., Poulton, S.W., Lyons, T.W., 2013. Large-scale fluctuations in Precambrian atmospheric and oceanic oxygen levels from the record of U in shales. Earth Planet. Sci. Lett. 369–370, 284–293.
Pašava, J., Kříbek, B., Dobeš, P., Vavřín, I., Žák, K., Delian, F., Tao, Z., Boiron, M., 2003. Tin-polymetallic sulfide deposits in the eastern part of the Dachang tin field (South China) and the role of black shales in their origin. Mineral. Deposita 38, 39–66.
Pašava, J., Kříbek, B., Vymazalová, A., Sýkorová, I., Žák, K., Orberger, B., 2008. Multiple sources of metals of mineralization in Lower Cambrian Black Shales of South China: evidence from geochemical and petrographic study. Resour. Geol. 58, 25–42.
Pašava, J., Tornos, F., Chrastný, V., 2014. Zinc and sulfur isotope variation in sphalerite from carbonate-hosted zinc deposits, Cantabria. Spain. Mineral. Deposita 49, 797–807.
Pašava, J., Chrastný, V., Loukola-Ruskeeniemi, K., Šebek, O., 2018. Nickel isotopic variation in black shales from Bohemia, China, Canada, and Finland: a reconnaissance study. Mineral. Deposita 54, 719–742.
Pokrovsky, O.S., Viers, J., Freydier, R., 2005. Zinc stable isotope fractionation during its adsorption on oxides and hydroxides. J. Colloid Interface Sci. 291, 192–200.
Samanta, M., Ellwood, M.J., Sinoir, M., Hassler, C.S., 2017. Dissolved zinc isotope cycling in the Tasman Sea, SW Pacific Ocean. Mar. Chem. 192, 1–12.
Scott, C., Lyons, T.W., 2012. Contrasting molybdenum cycling and isotopic properties in euxinic versus non-euxinic sediments and sedimentary rocks: refining the paleoproxies. Chem. Geol. 324–325, 19–27.
Shao, S.C., Li, C.Y., 1996. Metallogenetic rules of the strata-bound Pb-Zn deposit in Dengying Formation of the west margin of Yangtze massif and its possibility of ore-forming super-large ore deposit. Yunnan Geology 15, 345–350 (In Chinese with English abstract).
Steiner, M., Wallis, E., Erdtmann, B.D., Zhao, Y.L., Yang, R.D., 2001. Submarine hydrothermal exhalative ore layers in black shales from South China and associated fossils-insights into a Lower Cambrian facies and bio-evolution. Palaeogeogr. Palaeoclimatol. Palaeoecol. 169, 165–191.
Suhr, N., Schoenberg, R., Chew, D., Rosca, C., Widdowson, M., Kamber, B.S., 2018. Elemental and isotopic behaviour of Zn in Deccan basalt weathering profiles: chemical weathering from bedrock to laterite and links to Zn deficiency in tropical soils. Sci. Total Environ. 619–620, 1451–1463.
Tan, H., Wang, G.R., Lan, A.P., 2012. Geologic features and metallogenic regularity of Dujiaqiao lead-zinc deposit of Zhijin, Guizhou. Guizhou Geology 29, 169–172 (In Chinese with English abstract).
Tang, S.H., Zhu, X.K., Cai, J.J., Li, S.Z., He, X.X., Wang, J.H., 2006. Chromatographic separation of Cu, Fe and Zn using AG M P-1 anion exchange resin for isotope determination by MC-ICPMS. Rock and Mineral Analysis 25, 5–8 (in Chinese with English abstract).
Taylor, S.R., McLennan, S.M., 1985. The Continental Crust: Its Composition and Evolution. Blackwell, Oxford (312 pp.).
Tribovillard, N., Riboulleau, A., Lyons, T., Baudin, F., 2004. Enhanced trapping of molybdenum by sulfurized marine organic matter of marine origin in Mesozoic limestones and shales. Chem. Geol. 213, 385–401.
Tribovillard, N., Algeo, T.J., Lyons, T., Riboulleau, A., 2006. Trace metals as paleoredox and paleoproductivity proxies: an update. Chem. Geol. 232, 12–32.
Tribovillard, N., Algeo, T.J., Baudin, F., Riboulleau, A., 2012. Analysis of marine environmental conditions based on molybdenum–uranium covariation—applications to Mesozoic paleoceanography. Chem. Geol. 324–325, 46–58.
Vance, D., Little, S. H., Archer, C., Cameron, V., Andersen, M. B., and Rijkenberg, M. J. A., Lyons T.W., 2016, The oceanic budgets of nickel and zinc isotopes: the importance of sulfidic environments as illustrated by the Black Sea. Philos. Trans. R. Soc. A Math. Phys. Eng. Sci. 374, doi.org/https://doi.org/10.1098/rsta.2015.0294.
Veeramani, H., Eagling, J., Jamieson-hanes, J.H., Kong, L.Y., Ptacek, C.J., Blowes, D.W., 2015. Zinc isotope fractionation as an indicator of geochemical attenuation processes. Environ. Sci. Technol. Lett. 2, 314–319.
Wang, J., Li, Z.X., 2003. History of Neoproterozoic rift basins in South China: implications for Rodinia break-up. Precambrian Res. 122, 141–158.
Wen, H.J., Carignan, J., 2011. Selenium isotopes trace the source and redox processes in the black shale-hosted se-rich deposits in China. Geochim. Cosmochim. Acta 75, 1411–1427.
Wen, H., Carignan, J., Chu, X., Fan, H., Cloquet, C., Huang, J., Zhang, Y., Chang, H., 2014. Selenium isotopes trace anoxic and ferruginous seawater conditions in the Early Cambrian. Chem. Geol. 390, 164–172.
Wen, H.J., Fan, H.F., Zhang, Y.X., Cloquet, C., Carignan, J., 2015. Reconstruction of early Cambrian ocean chemistry from Mo isotopes. Geochim. Cosmochim. Acta 164, 1–16.
Wen, H.J., Zhou, Z.B., Liu, L., Qin, C.J., Huang, Y.C., Wen, X.Q., Shi, Q.P., Xu, D.P., Wang, W.J., 2017. The discovery of the Dahebian Pb Zn deposit in Tianzhu area of Guizhou Province and its prospecting significance. Geological Bulletin of China 36, 1288–1293 (In Chinese with English abstract).
Wilkinson, J.J., Weiss, D.J., Mason, T.F.D., Coles, B.J., 2005. Zinc isotope variation in hydrothermal systems: preliminary evidence from the Irish midlands ore field. Econ. Geol. 100, 583–590.
Xu, L.G., Lehmann, B., Mao, J.W., Qu, W.J., Du, A.D., 2011. Re-Os age of polymetallic Ni-Mo-PGE-Au mineralization in early Cambrian black shales of South China — a reassessment. Econ. Geol. 106, 511–522.
Xu, L.G., Lehmann, B., Mao, J.W., Nägler, T.F., Neubert, N., Böttcher, M.E., Escher, P., 2012. Mo isotope and trace element patterns of Lower Cambrian black shales in South China: multi-proxy constraints on the paleoenvironment. Chem. Geol. 318–319, 45–59.
Xu, L.G., Lehmann, B., Mao, J.W., 2013. Seawater contribution to polymetallic Ni–Mo–PGE–Au mineralization in Early Cambrian black shales of South China: evidence from Mo isotope, PGE, trace element, and REE geochemistry. Ore Geol. Rev. 52, 66–84.
Yin, R., Xu, L., Lehmann, B., Lepak, R.F., Hurley, J.P., Mao, J., Feng, X., Hu, R., 2017. Anomalous mercury enrichment in Early Cambrian black shales of South China: mercury isotopes indicate a seawater source. Chem. Geol. 467, 159–167.
Zhao, Y., Vance, D., Abouchami, W., De Baar, H.J.W., 2014. Biogeochemical cycling of zinc and its isotopes in the Southern Ocean. Geochim. Cosmochim. Acta 125, 653–672.
Zheng, Y., Anderson, R.F., van Geen, A., Kuwabara, J., 2000. Authigenic molybdenum formation in marine sediments: a link to pore water sulfide in the Santa Barbara Basin. Geochim. Cosmochim. Acta 64 (24), 4165–4178.
Zhou, J.X., 2010. Geochemistry of Dispersed Elements and Zinc Isotope in Carbonate-hosted Lead-Zinc Ore Deposits District, Northwest Guizhou Province, China Ph.D. Thesis. Guiyang (In Chinese with English abstract).
Zhou, Z.B., 2018. The Mineralization Regularity of Zinc-Lead Deposits in the Western Segment of Jiangnan Orogen Ph.D. Thesis. Guiyang (In Chinese with English abstract).
Zhou, J.X., Huang, Z.L., Zhou, M.F., Zhu, X.K., Muchez, P., 2014. Zinc, sulfur and lead isotopic variations in carbonate-hosted Pb–Zn sulfide deposits, Southwest China. Ore Geol. Rev. 58, 41–54.
Zhou, Z.B., Wen, H.J., Qin, C.J., Fourestier, J., Liu, L., Shi, Q.P., 2018. The genesis of the Dahebian Zn-Pb deposit and associated barite mineralization: implications for hydrothermal fluid venting events along the Nanhua Basin, South China. Ore Geol. Rev. 101, 785–802.